ARTICLE

Solution-Prepared Hybrid-Nanoparticle Dielectrics for High-Performance Low-Voltage Organic Thin-Film Transistors

Ye Gan,[†] Qin Jia Cai,[†] Chang Ming Li,* Hong Bin Yang, Zhi Song Lu, Cheng Gong, and Mary B. Chan-Park*

School of Chemical and Biomedical Engineering, Nanyang Technological University, 62 Nanyang Drive, Singapore 637459, Singapore

ABSTRACT Oleic acid capped barium strontium titanate (OA-BST) nanoparticles were synthesized for solution-prepared dielectrics in organic thin-film transistors (OTFTs). The as-synthesized nanoparticles were well-dispersed in organic solvents to deposit very homogeneous dielectric films by direct spin coating. Bottom-gate pentacene TFTs fabricated using these nanoparticle dielectric films showed high mobilities of 1−2 $cm^2\ V^{-1}\ s^{-1}$ with on/off ratios of 10^3 under a low driven voltage of −2.5 V. Top-gate poly(3,3‴-didodecylquaterthiophene) (PQT-12) TFTs with nanoparticle dielectrics also exhibited a low-voltage operation (−5 V) performance with mobilities of 0.01−0.1 $cm^2\ V^{-1}\ s^{-1}$ and on/off ratios of 10^3−10^4. Detailed studies on the gate voltage-dependent mobility of the devices showed that only a low gate electric field needed to achieve the saturated mobility for the OA-BST-based pentacene OTFTs could be attributed to the low trapped-state densities ($<3.9 \times 10^{11}\ cm^{-2}$) at the dielectric/semiconductor interfaces for these devices.

KEYWORDS: solution-processed • dielectrics • organic thin-film transistors • pentacene • trapped-state density

INTRODUCTION

Organic thin-film transistors (OTFTs) have been studied extensively for promising applications in large-area electronics at low cost (1). Great efforts have been made to improve the performance of OTFTs, which is generally benchmarked against that of amorphous silicon (a-Si) thin-film transistors (TFTs) with a field-effect mobility μ of ∼1 $cm^2\ V^{-1}\ s^{-1}$ (2). In OTFTs, semiconductor/dielectric pairs are essential for device performance because the charge transport is confined to several monolayers of semiconductor molecules at semiconductor/dielectric interfaces (3−6). Various dielectric materials, such as polymers (7−9), inorganic high-*k* materials (10, 11), and inorganic/polymer blends (12−15), have been incorporated into semiconductor/dielectric pairs for OTFTs; however, it still remains a great challenge for the dielectric materials to meet the requirements of solution processability, flexibility, low-voltage operation (≤10 V), and high charge mobility ($\mu \geq 1\ cm^2\ V^{-1}\ s^{-1}$).

One of the requirements for low-cost dielectric materials is solution processabilty. Researchers and engineers usually turn to polymeric materials, such as poly(vinylpyrrolidone) (PVP), polystyrene (PS), poly(methyl methacrylate) (PMMA), etc., which possess excellent solution processabilty and film flexibility but low dielectric constants (9). The low-power-consumption requirement can be met by employing inorganic thin films or solution-processed polymer/inorganic nanoblending or reducing the film thickness of the polymer to nanoscale. Inorganic thin films with large capacitance are usually deposited with vacuum systems at high cost. An anodization process becomes more attractive to produce pinhole-free metal oxide thin films at room temperature (10, 16, 17). However, the high-energy surfaces of the metal oxides are incompatible with the subsequent deposition of high-quality organic semiconductors (highly crystalline) (10, 11, 18). Polymer thin films in nanoscale thickness can be problematic because of a pinhole problem and need to be highly cross-linked. On the other hand, the homogeneous distribution of inorganic nanoparticles in a polymer matrix is very challenging. To ensure uniform and stable dielectric properties, dispersion of the inorganic nanoparticles is an important factor (19). An alternative approach for ultrathin and high-capacitance dielectrics is atomic layer deposition, which allows for deposition of highly conformal, defect-free dielectric layers on various substrates at relatively low temperature (20, 21). OTFTs with these dielectric materials generally gave field-effect mobility of less than 1 $cm^2\ V^{-1}\ s^{-1}$ at low-voltage operation (12, 15, 22). The low-voltage-driven and high-performance requirements for OTFTs are possibly associated with the trapped-state density at semiconductor/dielectric interfaces. At trapped sites such as Si−OH species at the semiconductor/dielectric interfaces, charge carriers may be trapped during transportation in the interface, leading to high-voltage-driven and poor device performance (23, 24). It has been reported that improvement of the field-effect mobility of the pentacene TFTs could be experimentally attributable to the reduction of the reactive sites at the interface, such as the alkylsilane treatment of the SiO_2 surface before pentacene deposition (25, 26).

* Corresponding author. E-mail: ecmli@ntu.edu.sg (C.M.L.), mbechan@ntu.edu.sg. (M.B.C.-P.).
Received for review June 4, 2009 and accepted August 31, 2009
[†] These authors contributed equally to this work.
DOI: 10.1021/am9003914

Published on Web 09/16/2009

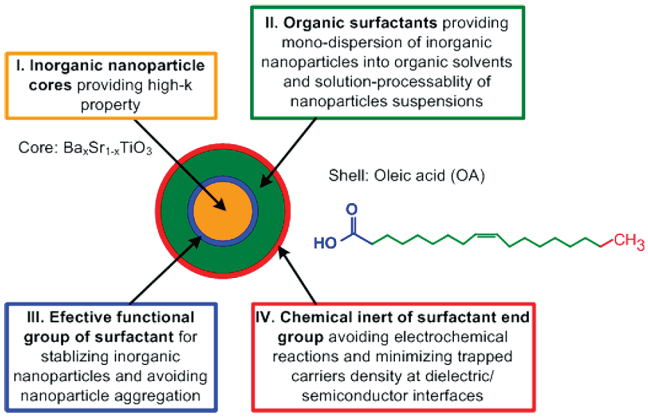

FIGURE 1. Schematic illustration of core−shell hybrid nanoparticles for dielectric application in OTFTs.

To fulfill the above requirements of dielectric materials for OTFTs, a novel dielectric material of an oleic acid capped barium strontium titanate (OA-BST) core−shell hybrid nanoparticle was designed and synthesized according to the following principles (as illustrated in Figure 1): (I) high-*k* inorganic nanoparticle cores can provide a high-*k* property, which facilitates charge accumulation in the channel; (II) organic surfactants, such as oleic acid, capping the surfaces of inorganic nanoparticle cores can enable well-dispersion of the inorganic nanoparticles in organic solvents and solution processability of nanoparticle suspensions; (III) effective functional groups of organic surfactants can stabilize the inorganic nanoparticles and avoid nanoparticles aggregation; (IV) the chemical inertness of the surfactant end group (pointing out from inorganic nanoparticle surfaces) may avoid possible electrochemical interactions and minimize the trapped-state density at the semiconductor/dielectric interfaces.

The OA-BST nanoparticles with a molar formula $Ba_xSr_{1-x}TiO_3$ in which x varies as 0.1, 0.2, and so on, until 0.9 mol %, were synthesized and characterized by high-resolution transmission electron microscopy (HRTEM) measurements. The nanoparticles were further well-dispersed in an organic solvent to fabricate uniform thin films by spin coating. The dielectric constants of the films with different Ba/Sr molar ratios of the nanoparticles were characterized. Bottom-gate pentacene and top-gate poly(3,3‴-didodecylquaterthiophene) (PQT-12) TFTs were fabricated using these nanoparticle dielectric films to investigate the electric transport performance. The gate voltage-dependent mobilities of these devices were studied to explore the possible mechanism of the electric transport at the dielectric/semiconductor interface.

EXPERIMENTAL SECTION

Materials. Barium oxide (97%), strontium oxide (99.9%), titanium isopropoxide (97%), diphenyl ether (99%), oleic acid (90%), ethylene glycol (99.8%, anhydrous), 2-propanol (99.9%), a 30% hydrogen peroxide solution in water, toluene (HPLC), pentacene (99.99%), and ethanol (≥99.8%) were obtained from Sigma-Aldrich and used as received without further purification. The poly(3,3‴-didodecylquaterthiophene) (PQT-12)/dichlorobenzene solution (0.3 wt %) was provided by Xerox Research Centre of Canada.

Synthesis of Oleic Acid Capped Barium Strontium Titanate (OA-BST). Barium titanium glycolate and strontium titanium glycolate complexes were prepared separately according to the literature (27). The two precursors of overall 5 mmol with systematically adjusted Ba^{2+}/Sr^{2+} molar ratios were transferred into a dry mixture of 50 mL of diphenyl ether and 5 mmol of stabilizing agent OA at 100 °C under an argon atmosphere. A total of 1.8 g of a 30 wt % hydrogen peroxide solution was injected slowly into the solution (vigorous exothermic reaction) to avoid a possible splashing hazard caused by boiling. The solution was maintained in a closed system and stirred at 100 °C over 48 h to promote further hydrolysis and the formation of the OA-capped nanoparticles. After the reaction, the solution was cooled to room temperature and the nanoparticles were readily precipitated with excess ethanol. The precipitate was washed six times with ethanol to remove absorbed OA with the assistance of a centrifuge.

Material Characterization. The surface properties of the dried nanoparticles were characterized by a Thermo Nicolet 5700 FTIR spectrometer, and the attenuated total reflectance Fourier transform infrared (ATR-FTIR) spectra were collected with a resolution of 1 cm^{-1}. The surface morphology and R_{rms} values were measured by an atomic force microscope (Digital Instruments Nanoscope IIIa MultiMode scanning probe microscope) in tapping mode with a scan rate of 0.5 Hz. The pentacene films were studies by X-ray diffraction (XRD) in the symmetric-reflection-coupled $\theta-2\theta$ arrangement. XRD patterns were recorded at room temperature on a Bruker AXS X-ray diffractometer using Cu Kα radiation ($\lambda = 1.5418$ Å).

Device Fabrication and Characterization. ***Capacitors.*** Metal−insulator−metal (MIM) capacitors of indium−tin oxide (ITO)/OA-BST nanoparticle film/Al were fabricated. OA-BST nanoparticle films were formed on ITO-coated glasses by spin coating of the nanoparticle suspensions in toluene (~40 mg/g). Silver top contacts of ~100 nm thickness and 4 mm^2 area were deposited on the nanoparticle films under 10^{-7} Torr. The capacitors were characterized using an HP 4284 Precision LCR meter.

Pentacene Transistors. Bottom-gate pentacene TFTs were fabricated by the thermal evaporation of pentacene films of 40 nm onto the OA-BST nanoparticle films on ITO/PET or Al/SiO_2 substrates under 10^{-7} Torr. Gold source-drain electrodes of 100 nm were subsequently defined on the pentacene films through a shadow mask. In addition, bottom-gate pentacene TFTs were also fabricated on a heavily doped n-type (n++) silicon wafer with a 100 nm top layer of SiO_2 as the insulator. The SiO_2 surfaces were treated with 10 mmol of an octyltrichlorosilane (OTS)/hexane solution for 30 min before pentacene deposition.

PQT-12 Transistors. PQT-12 TFTs were fabricated on an n++ silicon wafer with 100 nm thermally grown SiO_2 as the bottom-gate insulator. Gold/titanium (Au/Ti: 50 nm/1 nm) source-drain contacts were patterned using a lift-off technique. PQT-12 semiconductor layers of about 60 nm were deposited on OTS-treated substrates, subsequently annealed at 125 °C for 30 min, and cooled to room temperature in vacuum. The bottom-gate geometry was used to characterize the performance of PQT-12/OTS-SiO_2 TFTs. The top-gate devices were made by spin coating of OA-BST nanoparticle suspensions in toluene (~40 mg/g) on PQT-12 semiconductor layers, followed by deposition of ~100 nm silver on the nanoparticle dielectric films under 10^{-7} Torr as the top-gate electrode.

Transistor Characterizations. The electrical properties of the fabricated OTFTs were measured with a Cascade Microtech Summit 11751B-6 probe station and an Agilent 4157B semiconductor parameter analyzer.

RESULTS AND DISCUSSION

Figure 2a shows the HRTEM image of OA-$Ba_{0.1}Sr_{0.9}TiO_3$ nanoparticles, and the inset is the corresponding selected-

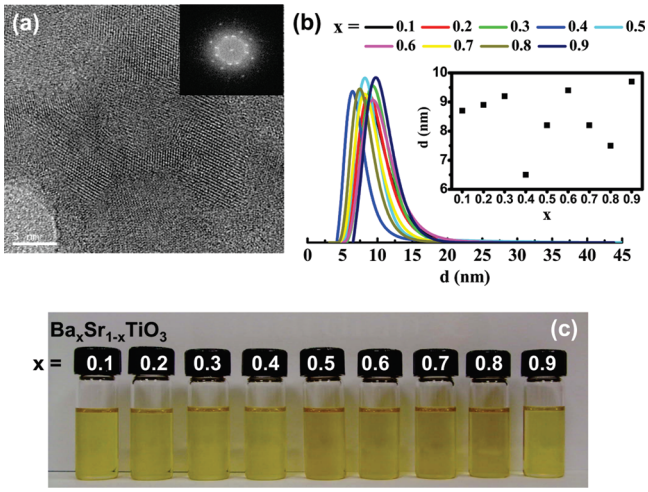

FIGURE 2. (a) HRTEM image of OA-$Ba_{0.1}Sr_{0.9}TiO_3$ nanoparticles. The inset is the corresponding SAED pattern. (b) OA-$Ba_xSr_{1-x}TiO_3$ nanoparticle size distribution from ζ-potential measurements. The inset is the mean size for different nanoparticles. (c) Digital images of clear OA-$Ba_xSr_{1-x}TiO_3$ nanoparticle suspensions in toluene (~40 mg/g), where $x = 0.1$, 0.2, and so on, until 0.9 from left to right.

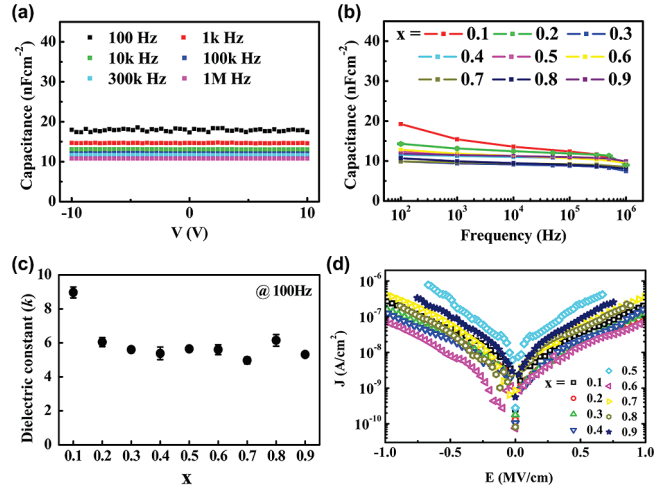

FIGURE 3. Electrical characteristics of spin-coated OA-BST nanoparticle films: (a) plots of capacitance versus voltage for the OA-$Ba_{0.1}Sr_{0.9}TiO_3$ film (~410 nm) at different frequencies; (b) plots of capacitance versus frequency in the range of 10^2–10^6 Hz for OA-BST films (380–510 nm); (c) comparison of k measured at 10^2 Hz; (d) current densities versus electric field plots.

area electron diffraction (SAED) pattern. Lattice structures can be observed and identified from the cores of the nanoparticles. The size of the nanoparticles is 5–8 nm. From ζ-potential measurements, the size of OA-$Ba_xSr_{1-x}TiO_3$ (x = 0.1, 0.2, ..., 0.9) nanoparticles is in the range of 6–10 nm, which is very close to the theoretical value in terms of the nanoparticle structure shown in Figure 2b. Figure 2c shows that very clear nanoparticle dispersions in nonpolar organic solvents (such as toluene) are produced. The dispersions are stable for more than 1 year without gelatinization or agglomerates. However, if the nanoparticles were dried, it would be hard for them to redisperse into the organic solvent, as discussed in our previous work (28). Thin films (300–400 nm thickness) obtained from spin coating of the nanoparticle suspensions are homogeneous and smooth, with a surface root-mean-square roughness (R_{rms}) ranging from 3.5 to 5.5 nm. The surfaces are hydrophobic with water contact angles of 93–105°.

It is known that the capacitance of a capacitor is more prominent at lower frequencies. The typical frequencies for characterizing the gate dielectric materials in organic transistors are in a range over 10^2–10^6 Hz (29, 30). The capacitance of the MIM capacitors was measured with a direct-current sweep voltage of ±10 V at fixed frequencies in the range of 10^2–10^6 Hz (Figure 3b), indicating that the capacitance only decreases slightly with an increase of the frequency. Figure 3a gives the relationship of capacitance versus voltage for the OA-$Ba_{0.1}Sr_{0.9}TiO_3$ film. No polarization behavior is observed for all OA-BST films. This is different from the highly crystallized pervoskite oxides that normally possess the ferroelectric property (31). The dielectric constant k values at 100 Hz calculated by $k = C_i t/\varepsilon_0$ (where ε_0, C_i, and t are the vacuum permittivity, unit area capacitance, and film thickness, respectively) for different OA-BST nanoparticles are shown in Figure 3c, indicating that OA-$Ba_{0.1}Sr_{0.9}TiO_3$ has a dielectric constant of ~9.6. With increasing Ba^{2+} loading with a reduction of the Sr^{2+} contents in the compound, k drops to 6.1 for OA-$Ba_{0.2}Sr_{0.8}TiO_3$ and then 5.6 for OA-$Ba_{0.3}Sr_{0.7}TiO_3$. Films with OA-$Ba_{0.4}Sr_{0.6}TiO_3$ to OA-$Ba_{0.9}Sr_{0.1}TiO_3$ exhibit dielectric constants in a range over 5–6. This result suggests that small differences in the Ba/Sr molar ratio of the nanoparticles at low values ranging from 0.1 to 0.4 can result in significant k changes of the nanoparticle films. The spin-coated OA-BST nanoparticle films (350–450 nm) show leakage current densities in the range of 10^{-8}–10^{-6} A cm^{-2} when the electric field across the capacitor is 0.7–1 MV cm^{-1} (Figure 3d).

Parts a and b of Figure 4 give a set of representative transfer curves for both forward and reverse gate bias scans (scan rate: ~0.7 V s^{-1}) and the $|I_D|^{1/2}$ vs V_G plots for the forward condition of bottom-gate pentacene TFTs and top-gate PQT-12 TFTs, respectively. Both bottom- and top-gate TFTs have selected OA-BST nanoparticles as gate dielectrics. The OA-BST-based pentacene TFTs exhibit the field-effect mobilities of 1–2 cm^2 V^{-1} s^{-1} with on/off ratios of 10^3 at the low operating voltage $V_D = V_G = -2.5$ V. PQT-12 TFTs operated under higher voltage $V_D = V_G = -5$ V have field-effect mobilities of 0.01–0.1 cm^2 V^{-1} s^{-1} and on/off ratios of 10^3. The corresponding output characteristics of the devices in Figure 4c clearly demonstrate the typical linear/saturation behavior. The hysteresis of I_D–V_G is observed (in Figure 4a) with a positive shift in V_{th} (ΔV_{th} = 0.6–0.9 V), probably due to the trapping of electrons injected from the gate (gate leakage) (32). Hysteresis is often observed in OTFTs with high-k polymeric dielectric materials, such as poly(vinyl alcohol) (33), polymer electrolyte (34), as well as sol–gel silica dielectrics (35), which is probably due to the trapping of electrons injected from the gate. The hysteresis can be suppressed effectively by lowering the scan rate (36).

The device mobility is known to be gate-voltage-dependent in OTFTs (3, 37). The dependency of the mobility of both pentacene and PQT-12 TFTs with OA-BST dielectrics on different gate voltages was studied to explore the fundamental insight of the OTFT mobility. For comparison, the

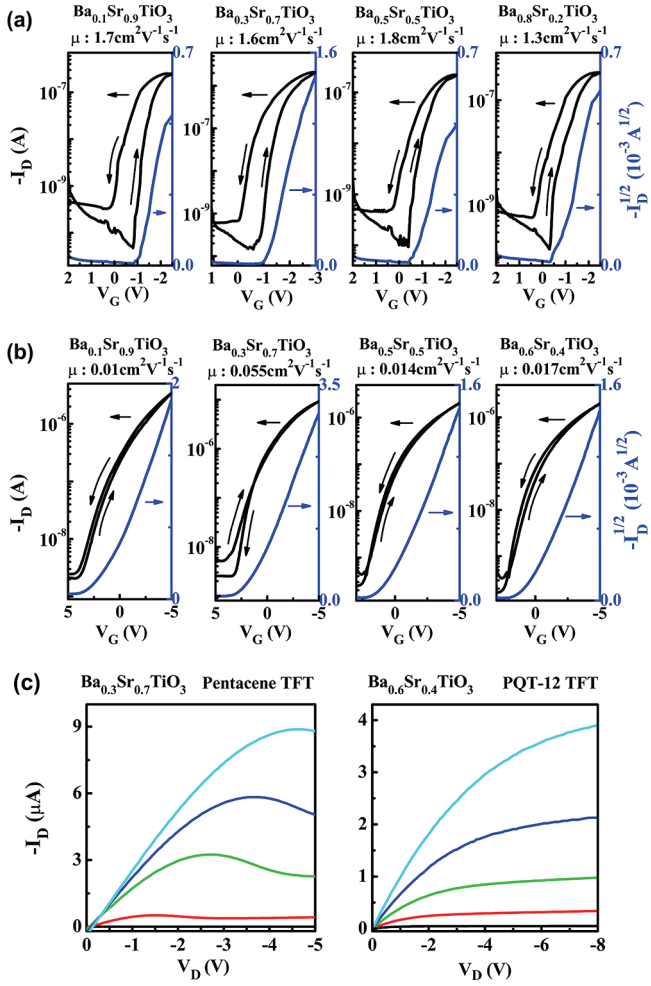

FIGURE 4. Representative transfer characteristics and $|I_D|^{1/2}$ vs V_G plots of OTFTs with OA-BST nanoparticle films as gate dielectrics. (a) Bottom-gate pentacene TFTs, channel width/length (W/L) = 11, 45, 13, and 20 for samples $Ba_{0.1}Sr_{0.9}TiO_3$ (21 nF cm^{-2}), $Ba_{0.3}Sr_{0.7}TiO_3$ (9.8 nF cm^{-2}), $Ba_{0.5}Sr_{0.5}TiO_3$ (16.1 nF cm^{-2}), and $Ba_{0.8}Sr_{0.2}TiO_3$ (16.8 nF cm^{-2}), respectively. (b) Top-gate PQT-12 TFTs, channel width/length (W/L) = 900 for $Ba_{0.1}Sr_{0.9}TiO_3$ (21.8nF cm^{-2}), $Ba_{0.3}Sr_{0.7}TiO_3$ (10.1 nF cm^{-2}), $Ba_{0.5}Sr_{0.5}TiO_3$ (12.8 nF cm^{-2}), and $Ba_{0.6}Sr_{0.4}TiO_3$ (12.7 nF cm^{-2}), respectively. (c) Output characteristics of the selected devices in parts a and b: for the bottom-gate pentacene TFT, the gate voltage increased from 0 to −4 V in steps of −1 V, and for the top-gate PQT-12 TFT, the gate voltage increased from 0 to −6.4 V in steps of −1.6 V, respectively.

investigations of this dependency were also conducted on devices with OTS-SiO_2 dielectrics. To minimize the gate stress effect, 5 min of rest was allowed between two consecutive measurements for each device. Normalized mobility was used to have a better image in which to display how the mobility varied with V_G for different devices by neglecting the mobility difference caused by the device variation. It was defined as the actual mobility at the corresponding V_G over the saturated (maximum) mobility obtained from the same device. The mobilities versus gate-voltage dependencies are plotted in Figure 5a,b for pentacene and PQT-12 TFTs, respectively. The saturated mobilities, together with other characteristics of the devices, are listed in Table 1. The pentacene/OA-BST TFTs all demonstrate a mobility plateau (1−3.5 cm^2 V^{-1} s^{-1}) at much lower driven voltages around −5 V compared to the pentacene/OTS-SiO_2

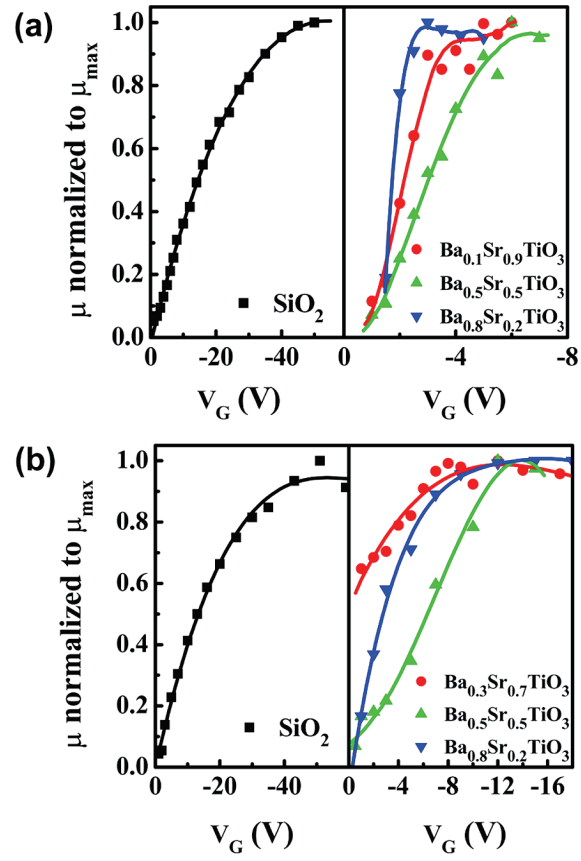

FIGURE 5. Gate-dependence mobility of the OTFTs with OA-BST nanoparticle films as gate dielectrics. (a) Bottom-gate pentacene TFTs, channel width/length (W/L) = 24, 11, 13, and 20 for samples OTS-SiO_2, OA-$Ba_{0.1}Sr_{0.9}TiO_3$, OA-$Ba_{0.5}Sr_{0.5}TiO_3$, and OA-$Ba_{0.8}Sr_{0.2}TiO_3$, respectively. (b) Top-gate PQT-12 TFTs, channel width/length (W/L) = 90, 180, 90, and 90 for samples OTS-SiO_2, OA-$Ba_{0.3}Sr_{0.7}TiO_3$, OA-$Ba_{0.5}Sr_{0.5}TiO_3$, and OA-$Ba_{0.8}Sr_{0.2}TiO_3$, respectively.

TFTs, where the mobility plateau is not observed even at the gate voltage of −50 V and the highest mobility is only ~0.5 cm^2 V^{-1} s^{-1}. It can be seen that the OA-BST-based pentacene TFTs exhibit superior performance over the pentacene TFTs on OTS-SiO_2. The morphology and crystallinity of the pentacene films on the respective substrates were examined using atomic force microscopy and XRD. The pentacene films illustrate a similar structure on OA-BST nanoparticle films and OTS-SiO_2 surfaces (Figure S1 in the Supporting Information). The mobility plateau occurs at a driven voltage of around −12 V for top-gate PQT-12/OA-BST TFTs (0.03−0.04 cm^2 V^{-1} s^{-1}), while taking place at a high operating voltage (−55 V) for the bottom-gate PQT-12/OTS-SiO_2 TFTs (~0.09 cm^2 V^{-1} s^{-1}). The lower device μ_{max} of the top-gate PQT-12 TFTs may be related to the high surface roughness of the PQT-12 films (38). Rougher semiconductor surfaces and probable moistures adsorbed at the interface during fabrication in an atmospheric environment could degrade the device mobility (39−41).

The dependency of field-effect mobility on the gate voltage could be described by a multiple trapping and release model (37, 42), which has been generally used to describe the charge-transport behavior in OTFTs. According to this model, there are two important factors significantly influencing the channel mobility: one is the number of charge

Table 1. Performance of Bottom-Gate Pentacene and Top-Gate PQT-12 TFTs

organic semiconductor	dielectric	dielectric thickness (nm)	μ_{max} ($cm^2\ V^{-1}\ s^{-1}$)	V_G (V)	C_i ($nF\ cm^{-2}$)	V_{th} (V)	S ($V\ dec^{-1}$)	N_{trap}^{max} (cm^{-2})
pentacene	OTS-SiO_2	100	0.54	−50	34	−9.8	0.778	2.06×10^{12}
	$Ba_{0.1}Sr_{0.9}TiO_3$	420	2.7	−5	21	−2.5	0.232	3.88×10^{11}
	$Ba_{0.5}Sr_{0.5}TiO_3$	330	3.42	−5	16.1	−1.14	0.216	2.7×10^{11}
	$Ba_{0.8}Sr_{0.2}TiO_3$	330	1.38	−3	16.8	−0.8	0.277	3.9×10^{11}
PQT	OTS-SiO_2	100	0.089	−55	34	−9	0.989	3.37×10^{12}
	$Ba_{0.3}Sr_{0.7}TiO_3$	505	0.04	−12	10.1	2.8	2.05	2.15×10^{12}
	$Ba_{0.5}Sr_{0.5}TiO_3$	420	0.03	−13	12.8	−0.73	1.26	1.64×10^{12}
	$Ba_{0.8}Sr_{0.2}TiO_3$	495	0.04	−12	11.3	0.4	1.08	1.23×10^{12}

carriers induced, which can be denoted as the unit area carrier charge (Q_s), and another is the number of trapped states to be filled. Usually, one is more concerned with the first factor because higher k insulators could achieve a sufficient number of charge carriers to fill all of the trapped states at lower gate voltages (42). Interestingly, in our experimental results, as shown in Table 1, the OA-BST dielectrics have a unit area capacitance of 10−21 nF cm^{-2}, which is much lower than those of the high-k materials (80 nm Al_2O_3, 90 nF cm^{-2} (3); 270 nm TiO_2/PVP/PαMS, 34.4 nF cm^{-2} (12); 250 nm ZrO_2-OTMS, ∼68 nF cm^{-2} (22); HfO_2, 0.69 μF cm^{-2} (43)) and even SiO_2 (100 nm: ∼34 nF cm^{-2}). The gate-voltage-accumulated charge carriers known to be confined very close to the semiconductor/insulator interfaces should be much smaller in the pentacene/OA-BST system than those dielectric systems reported for low-voltage high-performance devices (3, 12, 22, 43). However, the mobility of the pentacene/OA-BST TFTs is almost 1 order higher and under less than 1 order lower of the gate field (E). Very likely, the trapped-state densities at the semiconductor/insulator interfaces play the key role in the high-mobility and low-voltage performance of OA-BST-based pentacene devices.

The maximum interface trapped-state density can be estimated using $N_{trap}^{max} = (C_i/q)[(qS \log e/k_BT) - 1]$ (44, 45), where k_B, T, e, q, S, and C_i are Boltzmann's constant, the temperature, the base of the natural logarithm, the electron charge, the reciprocal subthreshold swing, and the dielectric capacitance per unit area, respectively. The calculated maximum trapped-state densities of the devices at the maximum mobility condition are also summarized in Table 1. Clearly, S and the threshold voltages (V_{th}) for the pentacene/OA-BST devices are much better than those for the pentacene/OTS-SiO_2 devices. The pentacene/OA-BST devices have maximum trapped-state densities in the range of $(2.7-3.9) \times 10^{11}$ cm^{-2}, almost 1 order lower than those for OTS-SiO_2 devices (2.06×10^{12} cm^{-2}). The top-gate PQT/OA-BST devices exhibit higher maximum trapped-state densities in the range of $(1-2) \times 10^{12}$ cm^{-2}, which could be the origin for the lower μ_{max} and higher subthreshold swings obtained on these devices as discussed above. However, these values are still less than those of bottom-gate PQT/OTS-SiO_2 devices (3×10^{12} cm^{-2}). Fundamentally, fewer numbers of charge carriers are needed to fill the localized states in the devices with low trapped-state densities, and low-voltage operation with high mobility could be achieved on the OA-BST dielectric-based OTFTs. In comparison to cross-linked PVP dielectric films with similar capacitance per unit area (10−20 nF cm^{-2}) (46) used in OTFTs, the OA-BST dielectrics have advantages of enabling much lower voltage for device operation. In addition, the dielectrics developed in this work do not need the postannealing for cross-linking required by the polymer-based ones. These results suggest that the trapped-state density at semiconductor/dielectric interfaces is important for enabling low-voltage high-performance OTFTs and should also be taken into consideration during the design of the proper dielectric materials for OTFTs.

In Figure 6a−j, the FTIR spectra of OA and OA-$Ba_xSr_{1-x}TiO_3$ nanoparticles for all samples display two strong peaks at 2922 and 2853 cm^{-1}, which are assigned to the intense antisymmetric and symmetric C−H stretching vibrations of the $-CH_2-$ groups in the hydrocarbon moiety (47). The weak absorption band at 3006 cm^{-1}, attributable to the olefinic C−H stretching vibration (48), is also clearly observable. The strong adsorption peak at 1708 cm^{-1} shown in Figure 6a, associated with free C═O stretching vibration, is absent in the spectra for OA-capped nanoparticles (Figure 6b−j), while two strong characteristic bands centered at 1550 and 1404 cm^{-1} appear in Figure 6b−j. These two absorption bands can be characteristically attributed to the COO− antisymmetric and symmetric stretching vibrations of carboxylate anions complexed with the metal surface (48, 49). The results suggest that OA as the stabilizing ligand is effectively bound to surfaces of the inorganic nanoparticle cores and nearly no free OA is present in the nanoparticle

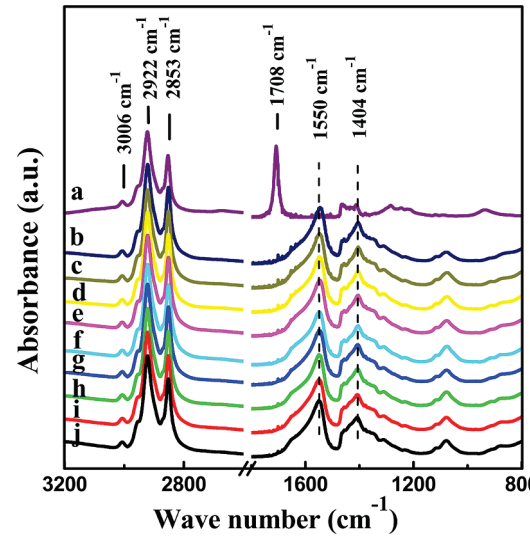

FIGURE 6. FTIR spectra of representative (a) OA and (b−j) OA-$Ba_xSr_{1-x}TiO_3$ nanoparticles where x = 0.1, 0.2, and so on, until 0.9.

suspensions. It has been shown that alkyl chains on modified dielectric surfaces can substantially reduce the interfacial trappes-state density (23, 50, 51), which is principally attributed to interfacial chemical functionalities/species such as Si−OH for SiO_2 dielectrics, in conjunction with adsorbed H_2O and adventitious carbon contamination (52, 53). It has been found that silanol groups cannot be completely removed by such self-assembled alkyl layers (54). On the other hand, the alkoxide precursors are readily reactive with carboxylic acids to produce OA-BST nanoparticles, thus resulting in significantly lower density of metal−OH species on the nanoparticle surfaces (55, 56). In addition, the near absence of −COOH groups on the nanoparticle surfaces could avoid possible electrochemical reactions and minimize the trapped-state density at the semiconductor/dielectric interface when the charge carriers are transported (26).

CONCLUSIONS

In summary, solution-processable OA-$Ba_xSr_{1-x}TiO_3$ nanoparticles, with x varying as 0.1, 0.2, and so on, until 0.9 mol %, were synthesized for dielectric applications in low-voltage OTFTs. The dielectric constant of the spin-on OA-BST films varied in the range from 5 to 9.6 with different Ba/Sr molar ratios in the nanoparticles. Bottom-gate pentacene and top-gate PQT-12 TFTs with the OA-BST films as gate insulators were fabricated. The studies on the gate dependence of mobility in the devices show that very high device mobilities (1.4−3.4 $cm^2\ V^{-1}\ s^{-1}$) could be obtained at low operating voltages (<−5 V) for pentacene TFTs. Low-operating voltages (∼−12 V) are also demonstrated on PQT-12 TFTs with a mobility of ∼0.1 $cm^2\ V^{-1}\ s^{-1}$ and on/off ratios of 10^3−10^4. This prominent device performance on the OA-BST nanoparticle dielectrics was investigated to be attributable to the very low trapped-state densities (<$3.9 \times 10^{11} cm^{-2}$) at the semiconductor/insulator interface, which was more than 1 order lower than that obtained in the OTS- SiO_2 devices.

Acknowledgment. This work is financially supported by Singapore A*STAR under Grant 052 117 0031.

Supporting Information Available: Surface morphologies and XRD patterns of pentacene films. This material is available free of charge via the Internet at http://pubs.acs.org.

REFERENCES AND NOTES

(1) Kelley, T. W.; Baude, P. F.; Gerlach, C.; Ender, D. E.; Muyres, D.; Haase, M. A.; Vogel, D. E.; Theiss, S. D. *Chem. Mater.* **2004**, *16* (23), 4413.
(2) Sirringhaus, H. *Adv. Mater.* **2005**, *17*, 2411.
(3) Kalb, W.; Lang, P.; Mottaghi, M.; Aubin, H.; Horowitz, G.; Wuttig, M. *Synth. Met.* **2004**, *146* (3), 279.
(4) Lim, S. C.; Kim, S. H.; Lee, J. H.; Kim, M. K.; Kim, D. J.; Zyung, T. *Synth. Met.* **2005**, *148* (1), 75.
(5) Yildirim, F. A.; Schliewe, R. R.; Bauhofer, W.; Meixner, R. M.; Goebel, H.; Krautschneider, W. *Org. Electron.* **2008**, *9* (1), 70.
(6) Tello, M.; Chiesa, M.; Duffy, C. M.; Sirringhaus, H. *Adv. Funct. Mater.* **2008**, *18*, 3907.
(7) Kim, C.; Facchetti, A.; Marks, T. J. *Science* **2007**, *318* (5847), 76.
(8) Kim, S. H.; Yang, S. Y.; Shin, K.; Jeon, H.; Lee, J. W.; Hong, K. P.; Park, C. E. *Appl. Phys. Lett.* **2006**, *89* (18), 183516.
(9) Kim, C.; Wang, Z.; Choi, H. J.; Ha, Y. G.; Facchetti, A.; Marks, T. J. *J. Am. Chem. Soc.* **2008**, *130*, 6867.
(10) Majewski, L. A.; Schroeder, R.; Grell, M.; Glarvey, P. A.; Turner, M. L. *J. Appl. Phys.* **2004**, *96* (10), 5781.
(11) Majewski, L. A.; Schroeder, R.; Grell, M. *Adv. Funct. Mater.* **2005**, *15* (6), 1017.
(12) Chen, F. C.; Chuang, C. S.; Lin, Y. S.; Kung, L. J.; Chen, T. H.; Shieh, H. P. D. *Org. Electron.* **2006**, *7* (5), 435.
(13) Hwang, D. K.; Lee, K.; Kim, J. H.; Im, S.; Kim, C. S.; Baik, H. K.; Park, J. H.; Kim, E. *Appl. Phys. Lett.* **2006**, *88*, (24).
(14) Lee, K. H.; Choi, J. M.; Im, S.; Lee, B. H.; Im, K. K.; Sung, M. M.; Lee, S. *Appl. Phys. Lett.* **2007**, *91* (12), 123502.
(15) Jung, C.; Maliakal, A.; Sidorenko, A.; Siegrist, T. *Appl. Phys. Lett.* **2007**, *90* (6), 062111.
(16) Tate, J.; Rogers, J. A.; Jones, C. D. W.; Vyas, B.; Murphy, D. W.; Li, W. J.; Bao, Z. A.; Slusher, R. E.; Dodabalapur, A.; Katz, H. E. *Langmuir* **2000**, *16* (14), 6054.
(17) Jeong, Y. T.; Dodabalapur, A. *Appl. Phys. Lett.* **2007**, *91* (19), 193509.
(18) Majewski, L. A.; Schroeder, R.; Grell, M. *Adv. Mater.* **2005**, *17*, 192.
(19) Dang, Z. M.; Lin, Y. Q.; Xu, H. P.; Shi, C. Y.; Li, S. T.; Bai, J. B. *Adv. Funct. Mater.* **2008**, *18* (10), 1509.
(20) Cao, Q.; Xia, M. G.; Shim, M.; Rogers, J. A. *Adv. Funct. Mater.* **2006**, *16* (18), 2355.
(21) Zhang, X. H.; Domercq, B.; Wang, X.; Yoo, S.; Kondo, T.; Wang, Z. L.; Kippelen, B. *Org. Electron.* **2007**, *8* (6), 718.
(22) Kim, J. M.; Lee, J. W.; Kim, J. K.; Ju, B. K.; Kim, J. S.; Lee, Y. H.; Oh, M. H. *Appl. Phys. Lett.* **2004**, *85* (26), 6368.
(23) Yoon, M. H.; Kim, C.; Facchetti, A.; Marks, T. J. *J. Am. Chem. Soc.* **2006**, *128* (39), 12851.
(24) Chua, L. L.; Zaumseil, J.; Chang, J. F.; Ou, E. C. W.; Ho, P. K. H.; Sirringhaus, H.; Friend, R. H. *Nature* **2005**, *434* (7030), 194.
(25) Kim, C. S.; Jo, S. J.; Lee, S. W.; Kim, W. J.; Baik, H. K.; Lee, S. J. *Adv. Funct. Mater.* **2007**, *17* (6), 958.
(26) Chua, L. L.; Zaumseil, J.; Chang, J. F.; Ou, E. C. W.; Ho, P. K. H.; Sirringhaus, H.; Friend, R. H. *Nature* **2005**, *434* (7030), 194–199.
(27) Day, V. W.; Eberspacher, T. A.; Frey, M. H.; Klemperer, W. G.; Liang, S.; Payne, D. A. *Chem. Mater.* **1996**, *8* (2), 330.
(28) Cai, Q. J.; Gan, Y.; Chan-Park, M. B.; Yang, H. B.; Lu, Z. S.; Song, Q. L.; Li, C. M.; Dong, Z. L. *Appl. Phys. Lett.* **2008**, *93* (11), 113304.
(29) Yoon, M. H.; Yan, H.; Facchetti, A.; Marks, T. J. *J. Am. Chem. Soc.* **2005**, *127* (29), 10388–10395.
(30) Acton, O.; Ting, G.; Ma, H.; Ka, J. W.; Yip, H. L.; Tucker, N. M.; Jen, A. K. Y. *Adv. Mater.* **2008**, *20* (19), 3697.
(31) Huang, L. M.; Chen, Z. Y.; Wilson, J. D.; Banerjee, S.; Robinson, R. D.; Herman, I. P.; Laibowitz, R.; O'Brien, S. *J. Appl. Phys.* **2006**, *100* (3), 034316.
(32) Huang, C.; West, J. E.; Katz, H. E. *Adv. Funct. Mater.* **2007**, *17* (1), 142.
(33) Lee, C. A.; Park, D. W.; Jin, S. H.; Park, I. H.; Lee, J. D.; Park, B. G. *Appl. Phys. Lett.* **2006**, *88* (25), 252102.
(34) Panzer, M. J.; Newman, C. R.; Frisbie, C. D. *Appl. Phys. Lett.* **2005**, *86* (10), 103503.
(35) Cahyadi, T.; Tan, H. S.; Mhaisalkar, S. G.; Lee, P. S.; Boey, F.; Chen, Z. K.; Ng, C. M.; Rao, V. R.; Qi, G. J. *Appl. Phys. Lett.* **2007**, *91* (24), 242107.
(36) Cai, Q. J.; Gan, Y.; Chan-Park, M. B.; Yang, H. B.; Lu, Z. S.; Li, C. M.; Guo, J.; Dong, Z. L. *Chem. Mater.* **2009**, *21* (14), 3153–3161.
(37) Mottaghi, M.; Horowitz, G. *Org. Electron.* **2006**, *7* (6), 528–536.
(38) Zhao, N.; Botton, G. A.; Zhu, S. P.; Duft, A.; Ong, B. S.; Wu, Y. L.; Liu, P. *Macromolecules* **2004**, *37* (22), 8307.
(39) Zhang, J.; Li, C. M.; Chan-Park, M. B.; Zhou, Q.; Gan, Y.; Qin, F.; Ong, B.; Chen, T. *Appl. Phys. Lett.* **2007**, *90* (24), 243502.
(40) Ling, M. M.; Bao, Z. N.; Li, D. W. *Appl. Phys. Lett.* **2006**, *88* (3), 033502.
(41) Veres, J.; Ogier, S.; Lloyd, G.; de Leeuw, D. *Chem. Mater.* **2004**, *16* (23), 4543.
(42) Dimitrakopoulos, C. D.; Purushothaman, S.; Kymissis, J.; Callegari, A.; Shaw, J. M. *Science* **1999**, *283* (5403), 822.
(43) Acton, O.; Ting, G.; Ma, H.; Ka, J. W.; Yip, H. L.; Tucker, N. M.; Jen, A. K. Y. *Adv. Mater.* **2008**, *20* (19), 3697.
(44) McDowell, M.; Hill, I. G.; McDermott, J. E.; Bernasek, S. L.; Schwartz, J. *Appl. Phys. Lett.* **2006**, *88* (7), 073505.
(45) Unni, K. N. N.; Dabos-Seignon, S.; Nunzi, J. M. *J. Mater. Sci.* **2006**, *41* (2), 317–322.
(46) Klauk, H.; Halik, M.; Zschieschang, U.; Schmid, G.; Radlik, W.; Weber, W. *J. Appl. Phys.* **2002**, *92* (9), 5259–5263.

(47) Pretsch, E.; Bühlmann, P.; Affolter, C. *Structure Determination of Organic Compounds—Tables of Spectral Data*, 3rd ed.; Springer-Verlag: New York, 2003.
(48) Thistlethwaite, P. J.; Hook, M. S. *Langmuir* **2000**, *16*, 4993.
(49) Nara, M.; Torii, H.; Tasumi, M. *J. Phys. Chem.* **1996**, *100* (51), 19812.
(50) Kobayashi, S.; Nishikawa, T.; Takenobu, T.; Mori, S.; Shimoda, T.; Mitani, T.; Shimotani, H.; Yoshimoto, N.; Ogawa, S.; Iwasa, Y. *Nat. Mater.* **2004**, *3* (5), 317.
(51) Salleo, A.; Chabinyc, M. L.; Yang, M. S.; Street, R. A. *Appl. Phys. Lett.* **2002**, *81* (23), 4383.
(52) Alexandrova, S.; Szekeres, A. *Phys. Status Solidi A* **2001**, *187* (2), 499.
(53) Smith, J. W. H.; Hill, I. G. *J. Appl. Phys.* **2007**, *101* (4), 044503-6.
(54) Angst, D. L.; Simmons, G. W. *Langmuir* **1991**, *7* (10), 2236.
(55) Cozzoli, P. D.; Kornowski, A.; Weller, H. *J. Am. Chem. Soc.* **2003**, *125* (47), 14539.
(56) O'Brien, S.; Brus, L.; Murray, C. B. *J. Am. Chem. Soc.* **2001**, *123*, 12085.

AM9003914